THE JOURNAL OF PHYSICAL CHEMISTRY LETTERS
A JOURNAL OF THE AMERICAN CHEMICAL SOCIETY

pubs.acs.org/JPCL

Letter

Insights into the Formation of Hydroxyl Radicals with Nonthermal Vibrational Excitation in the Meinel Airglow

Qixin Chen, Xixi Hu,* Hua Guo, and Daiqian Xie

Cite This: *J. Phys. Chem. Lett.* 2021, 12, 1822−1828

Read Online

ACCESS | Metrics & More | Article Recommendations

ABSTRACT: To understand night time airglow in the Meinel bands and heat conversion from the highly excited OH radicals in the upper atmosphere via the important atmospheric reaction H + O_3 → OH + O_2, we report here a quasi-classical trajectory study of the reaction dynamics on a recently developed full-dimensional potential energy surface (PES). Our results indicate that the reaction energy of this highly exoergic reaction is almost exclusively channeled into the vibration of the OH product, underscoring an extreme departure from the statistical limit. The calculated OH vibrational distribution is highly inverted and peaks near the highest accessible vibrational state, in excellent agreement with experimental observations, validating the accuracy of the PES. More importantly, the dynamical origin of the nonthermal excitation of the OH vibrational mode is identified by its large projection onto the reaction coordinate at a small potential barrier in the entrance channel, which controls the energy flow into various degrees of freedom in the products.

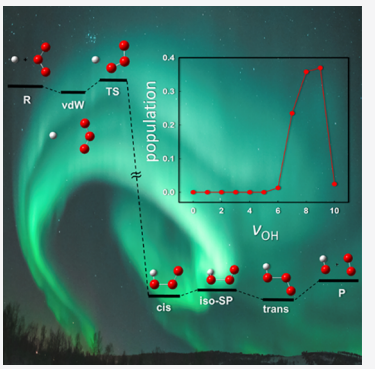

Downloaded via NANJING UNIV on February 18, 2021 at 00:32:55 (UTC).
See https://pubs.acs.org/sharingguidelines for options on how to legitimately share published articles.

Ever since its first discovery by Angström in 1868, airglow in the night sky has fascinated scientists for more than 100 years. It is now well established that the nightglow stems from visible photons emitted by highly excited atoms and molecules formed in the upper atmosphere via either chemical reactions or by cosmic rays. For instance, the hydroxyl nightglow in the Meinel bands is believed to stem from spontaneous emissions of highly vibrationally excited OH radicals[1,2] formed in the $H(^2S) + O_3(X^1A_1) \rightarrow OH(X^2\Pi) + O_2(X^3\Sigma_g^-)$ reaction.[3,4] The chemiluminescence is facilitated by a strongly inverted vibrational distribution in the OH product, which is uncommon for most chemical reactions. A complete understanding of the OH nightglow thus demands knowledge on how the vibrationally excited OH product is formed. In addition, this reaction is one of the dominant exothermic reactions that convert chemical potential energy into heat in the mesosphere. Radiative relaxation of the nonthermal OH radical in the Meinel bands competes with heat release via collisional quenching of OH(v) by O_2, N_2, and O. The kinetic modeling of the heating efficiency also requires the nascent distribution of the OH vibration.[5]

In the past several decades, several experiments have been performed to measure the nascent vibrational distribution of the OH radical produced in the H + O_3 → OH + O_2 reaction. In a pioneering study in 1968, Anlauf et al. used an experimental method based on infrared chemiluminescence to determine the vibrationally specific rates of the reaction. By converting spectral intensities to populations using calculated Einstein coefficients, these authors found that the OH product is excited up to v = 9.[6] However, the results from these experiments showed strong pressure dependence, due apparently to vibrational relaxation of the OH radicals. Emissions from OD were also reported for the D + O_3 reaction. In 1971, Charters et al. improved the measurement by using Fourier transform spectroscopy at low pressures in an attempt to minimize vibrational relaxation. Their results suggested that the OH radical was formed with an inverted vibrational distribution with the peak near the highest accessible vibrational state (v = 9).[7] However, the relaxation of vibrationally excited OH and its secondary reactions in this system have been shown to be very fast,[8,9] which might still impact the chemiluminescence experiment of Charters et al. Later, Ohoyama et al. investigated the same process under single-collision conditions using crossed molecular beams, which avoided energy transfer and secondary reactions.[10] These authors confirmed the inverted OH vibrational distribution with a peak at v = 9 and found little population below v = 4. Interestingly, they observed no OD chemiluminescence for the D + O_3 → OD + O_2 reaction in the wavelength range of 650 to 900 nm at flow rates of 15.0 and 2.0 μmol/s for deuterium and ozone, respectively. Therefore, no estimate for the nascent vibration distribution of the OD product was possible. The latest experiment was carried out by Klenerman and Smith in 1987. They measured

Received: January 16, 2021
Accepted: February 10, 2021

© XXXX American Chemical Society

https://dx.doi.org/10.1021/acs.jpclett.1c00159
J. Phys. Chem. Lett. 2021, 12, 1822−1828

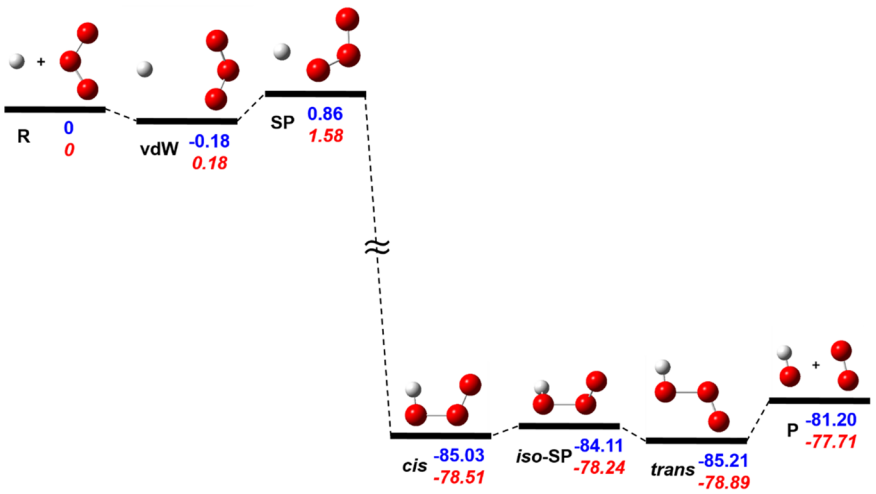

Figure 1. Energetics of the H + O_3 → OH + O_2 reaction on the $HO_3(X^2A'')$ PES. The energies are relative to the H + O_3 asymptote in kcal/mol. The blue values are energies of stationary points obtained from the PES, and their corrections with ZPE are shown in red italics.

the OH vibrational distribution based on infrared chemiluminescence using an interferential spectrometer by selection of amplitude modulation (SISAM), which can record the weak infrared chemiluminescent spectra emitted by reaction products under conditions of arrested relaxation.[11] Their experiment further confirmed the inverted OH vibrational distribution and the population ratios are in good agreement with those of Charters et al. when the same Einstein coefficients were used. Despite quantitative differences in the aforementioned experiments, all suggested an inverted vibrational distribution for OH, which peaks near v = 9. This is quite remarkable, because it implies that the reaction energy release ($\Delta H_{rxn}{}^0$ = 77.72 ± 0.06 kcal/mol)[12−14] is almost exclusively channeled into the OH vibrational mode, a far cry from the statistical limit where the energy release is equally partitioned into all product degrees of freedom (DOFs).[15] This unique feature of the reaction begs the question about the dynamical origin of the energy disposal.

This nonstatistical character of the reaction implicates a dynamic bottleneck which controls the energy flow. To gain insight into the experimental observations, it is necessary to understand the reaction dynamics and how it leads to the extremely nonthermal OH vibrational excitation. To this end, two potential energy surfaces (PESs) based on the double many-body expansion (DMBE) strategy have been developed by Varandas and co-workers at the UCISD/6-311G++(d, p) and QCISD(T)/CBS level of theory, respectively (called DMBE I PES and DMBE II PES).[16,17] The DMBE II PES is essentially the same in the rate-limiting region of the earlier DMBE I PES, with improvements in the HO_3 complex region. Unfortunately, the calculated OH vibrational distribution obtained on the DMBE I PES using the quasi-classical trajectory (QCT) method significantly underestimated the OH vibrational excitation determined by the latest experiments. Hence, these pioneering theoretical studies have provided limited insight into the origin of the OH vibrational excitation.

Ideally, reaction dynamics, particularly those affected by quantum effects, should be characterized by a quantum mechanical method,[18] but such calculations are still beyond the current computational capability due to the large exoergicity of the reaction and the involvement of three heavy atoms. In this work, we use the QCT method, which is much more efficient and reasonably accurate for the dynamics. The neglect of tunneling is expected to have a limited impact on the product state distribution, and the vibrational quantization in the products is effectively dealt with using a binning method with a "quantum spirit", associated with the Einstein-Brillouin-Keller (EBK) approach.[19]

In this Letter, we report a detailed QCT dynamic study of the H/D + O_3 reactions on a highly accurate PES recently constructed from a large number of multireference configuration interaction (MRCI) points using the high-fidelity permutation invariant polynomial-neural network (PIP-NN) method.[20,21] The MRCI treatment of the PES is essential due to the multireference nature of this system. Indeed, this PES has been shown to reproduce accurately the reaction kinetics of the H + O_3 reaction.[22] Dynamical calculations that for the first time yield the highly inverted OH vibrational distribution peaked at the highest accessible vibrational state are in much better agreement with experiment[7,10,11] than the previous theoretical study.[17] Moreover, we identified the underlying dynamical mechanism for the extreme OH vibrational excitation using a simple transition-state based model,[23,24] which provides a rational interpretation of the nonstatistical origin of the energy disposal in this reaction.

Figure 1 displays the energetics of the ground state $HO_3(^2A'')$ PES, including all calculated geometries and energies of stationary points along the H + O_3 → OH + O_2 reaction pathway. It is clear that the reaction is highly exoergic, with a reaction energy of 77.71 kcal/mol with zero point energy (ZPE) corrections, which, in principle, allows the population of the v = 9 vibrational state for OH and v = 12 for OD. Including the initial translation and rotation thermal energies, the highest accessible level is v = 10 for OH and v = 13 for OD. The *cis*- and *trans*-HOOO wells are separated with a small barrier, and these features are not expected to impact the dynamics in a significant way, thanks to their low energies relative to the reactant asymptote. In the entrance channel, there is a transition state (TS), lying 0.86 kcal/mol above the reactant asymptote,[20] which was shown to control the kinetics, particularly on the temperature dependence of the rate coefficient.[22] As discussed below, it also plays a key role in determining the energy disposal in the reaction. In addition, there is also a very shallow van der Waals well before the system reaches the TS.

https://dx.doi.org/10.1021/acs.jpclett.1c00159
J. Phys. Chem. Lett. 2021, 12, 1822−1828

Table 1. Energy Partition in Different DOFs of the Products at 150, 298, and 640 K

	$H + O_3$			$D + O_3$		
	150 K	298 K	640 K	150 K	298 K	640 K
f_{trans}	9.22%	10.03%	12.29%	7.42%	8.43%	11.25%
f_{rot}(OH/OD)	3.32%	3.61%	4.61%	3.97%	3.94%	4.64%
$f_{rot}(O_2)$	0.51%	0.82%	1.54%	0.47%	0.84%	1.54%
f_{vib}(OH/OD)	85.71%	83.22%	77.37%	87.00%	84.86%	79.11%
$f_{vib}(O_2)$	1.23%	2.33%	4.19%	1.14%	1.92%	3.47%

As discussed above, the H/D + O_3 reaction is highly exoergic. The calculated product energy disposal in different DOFs is presented in Table 1. It is clear that the OH/OD vibrational degree of freedom receives the lion's share (~80%) of the available energy, the energy disposal thus being highly nonstatistical, but this dominance decreases somewhat with temperature.

The calculated vibrational distributions for the product molecules OH and OD at 150 K are shown in the Figure 2 via two different binning methods, namely, the histogram binning (HB) and Gaussian binning (GB).[31,32] The vibrational distributions are inverted for both OH and OD, with almost no population below $v = 5$. The peak of the calculated OH vibrational distribution is at $v = 8$ for HB and $v = 9$ for GB. For comparison, the measured OH distributions[7,10,11] are also included in Figure 2(a) along with the theoretical result of Yu and Varandas,[17] which peaks at $v = 5$. It is clear from the figure that the agreement of our result with experiment is excellent, representing a substantial improvement over the previous theory. In addition, the GB method yields a better agreement with experiment than the HB method. For OD, as mentioned above, there is no reliable experimental data, as the only report is now known to be contaminated by vibrational relaxation.[6] Like in the OH case, our distribution peaks at $v = 12$, also significantly hotter than that of Yu and Varandas.[17] In Table 2, the nascent OH populations are listed for different temperatures. As shown in the table, the temperature dependence is relatively weak. In the same table, the vibration specific rate coefficients are also listed, which can be used in the modeling of energy transfer from OH(v) with other atoms and molecules. These state resolved rate coefficients are obtained by the following expression: $k(T, v) = k_{RPMD}(T)f(T, v)$, where the total rate coefficient $k_{RPMD}(T)$ is from our recent calculations[22] using the ring-polymer molecular dynamics (RPMD) method,[25−27] and $f(T, v)$ are from the fractions in Table 1.

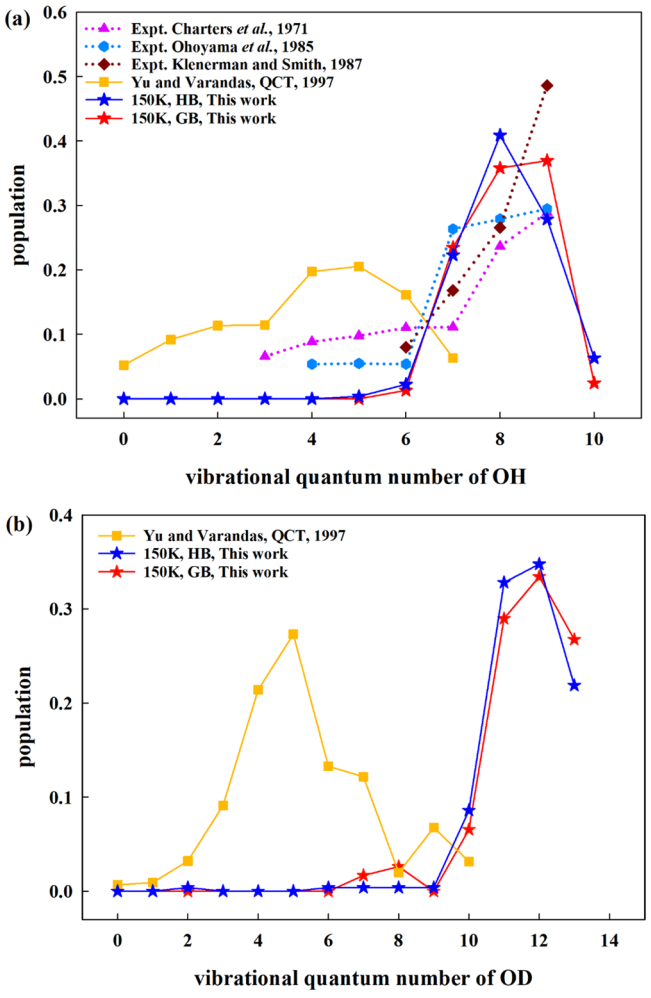

Figure 2. Calculated vibrational distributions of the products OH (a) and OD (b) compared with the available experiment results.

The poor agreement between the theoretical distribution of Yu and Varandas[17] and experiment is likely due to inaccuracies in their DMBE I PES.[16] In sharp contrast to our PIP-NN PES, which has a barrier of 0.86 kcal/mol, the DMBE I PES has a submerged saddle point, which is 0.48 kcal/mol below the reactant asymptote. This difference in this key point, which has been shown to result in very different rate coefficients,[22] suggests that the DMBE I PES might not be quantitatively accurate, presumably due to the multireference effects not included in their ab initio calculations. Indeed, the quantitative reproduction of both the rate coefficient and OH product vibrational distribution offers strong evidence in support of the accuracy of the PIP-NN PES and its underlying MRCI calculations.

The nascent vibrational distribution of the O_2 product at 150 K is also shown in Figure 3 for both H + O_3 and D + O_3 reactions. The vibration of the O_2 molecule is quite cold and insensitive to the isotope substitution, consistent with the fractions in Table 1. Specifically, the distributions decay monotonically with the vibrational quantum number, and they are only quantitatively different from different binning methods.

Figure 4(a) shows the rotational distributions of OH and OD at 150 K, which peak near $j = 3$ for both isotopologues, while the highest level peaks at $j = 18$. This is consistent with the experimental estimation that only 3% of the total released energy goes into OH rotation.[7] The rotational distribution of O_2 is shown in Figure 4(b). Note that only the *ortho* (odd j) states are populated for $^{16}O_2$, due to nuclear spins, so no *para* (even j) state population is included in the figure.

https://dx.doi.org/10.1021/acs.jpclett.1c00159
J. Phys. Chem. Lett. 2021, 12, 1822−1828

Table 2. Vibrational Distribution of the OH Product (v = 5−9) and Vibrational State Specific Rate Coefficients ($cm^3\ s^{-1}$) at Different Temperatures

	150 K	220 K	298 K	360 K	480 K	640 K
v = 9	0.37	0.33	0.33	0.27	0.27	0.24
v = 8	0.36	0.34	0.30	0.31	0.28	0.30
v = 7	0.23	0.28	0.27	0.33	0.28	0.25
v = 6	0.01	0.05	0.05	0.05	0.07	0.07
v = 5	0.00	0.00	0.00	0.01	0.02	0.03
k_{RPMD}	5.49×10^{-12}	9.37×10^{-12}	1.61×10^{-11}	2.43×10^{-11}	4.00×10^{-11}	6.67×10^{-11}

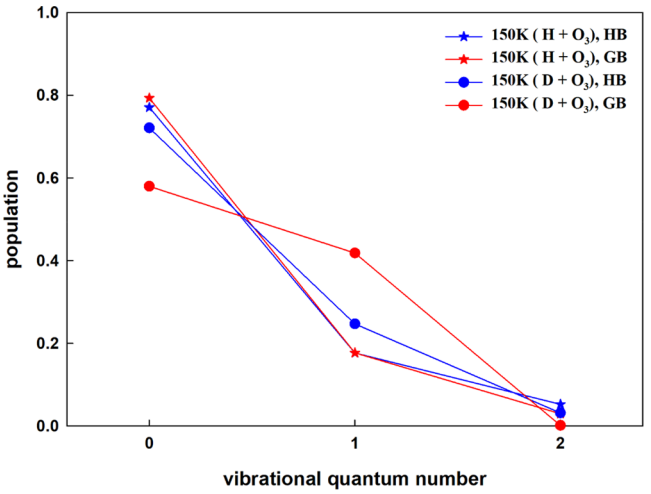

Figure 3. Vibrational state distributions of the O_2 product at 150 K.

To gain insight into the mode specific energy disposal in the product DOFs presented above, we examine the TS in the entrance channel. The attack of a terminal oxygen of the O_3 reactant by H leads to a *cis*-HOOO saddle point, as shown in Figure 1. The H−O distance at the SP is 2.024 Å, which is significantly larger than that in the OH product (0.972 Å). This large difference is presumably responsible for its strong vibrational excitation in the OH product. On the other hand, the remaining O_2 serves essentially as a spectator, as the O−O bond length in O_3, the TS, and O_2 is essentially the same, leading to minor vibrational excitation in the O_2 product. Furthermore, the post-TS PES exerts a weak torque on the two departing diatoms, resulting in minor rotational excitation. This picture helps to identify the dynamic origin of the extreme OH vibrational excitation.

To provide a more quantitative picture, we invoke the sudden vector projection (SVP) model,[23,24] which can be considered as an extension of Polanyi's rules.[28] The SVP model assumes the formation of the products is a fast process, and the product mode that couples strongly with the reaction coordinate at the TS receives most of the energy release and *vice versa*. Denoting $\vec{Q}_i$ as the ith normal mode vector of the product and $\vec{Q}_{RC}$ to the reaction coordinate at the TS, the coupling strength of the two can be represented as the projection of $\vec{Q}_i$ onto $\vec{Q}_{RC}$: $P_i = \vec{Q}_i \cdot \vec{Q}_{RC} \in [0, 1]$. The projection value thus reflects the efficacy for energy disposal in the sudden limit. The results of the SVP model (Table 3) show that the OH/OD vibration shows a strong coupling with the reaction coordinate, while all other modes are only weakly coupled with the reaction coordinate. The fact that the reaction coordinate at the TS is dominated by the O−H (O−D) vibration predicts a near exclusive energy disposal to the vibrational mode of the OH/OD product, consistent with the QCT results.

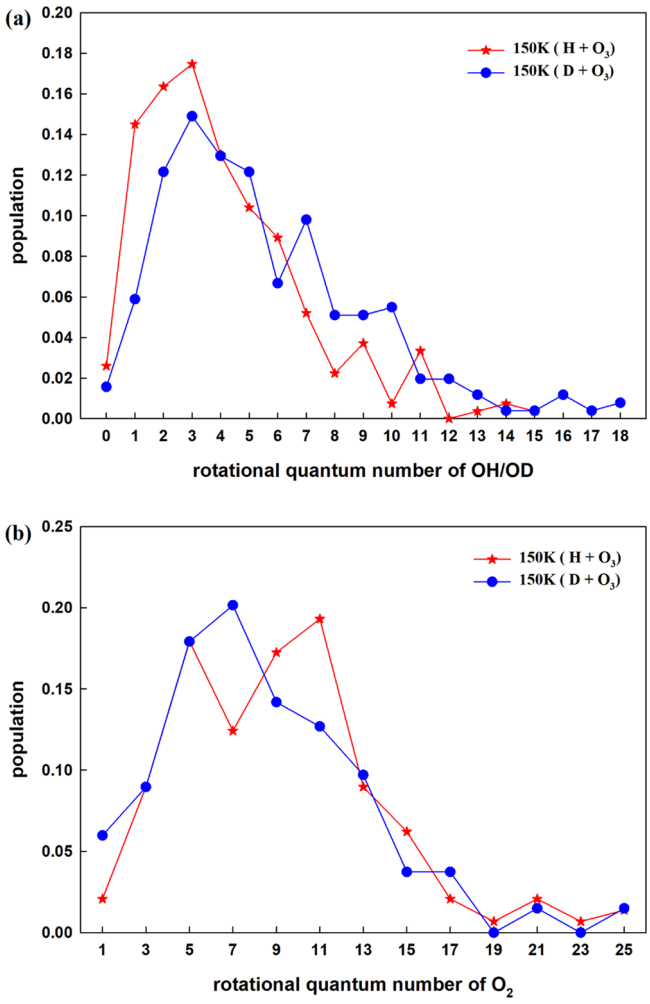

Figure 4. Rotational state distributions of the OH/OD (a) and O_2 (b) products at 150 K.

Table 3. SVP Projections for the Product Modes of the H/D + O_3 → OH/OD + O_2 Reaction

species	mode	H + O_3	D + O_3
product	relative translation	0.071	0.042
OH/OD	rotation	0.022	0.010
O_2	rotation	0.026	0.009
OH/OD	stretch	0.988	0.992
O_2	stretch	0.030	0.025

To gain further insight into the microscopic reaction mechanism, we have examined the dynamics in more detail.

https://dx.doi.org/10.1021/acs.jpclett.1c00159
J. Phys. Chem. Lett. 2021, 12, 1822−1828

Figure 5(a) shows a typical reactive trajectory for the reaction. For this trajectory at a relative translational energy of 4.94

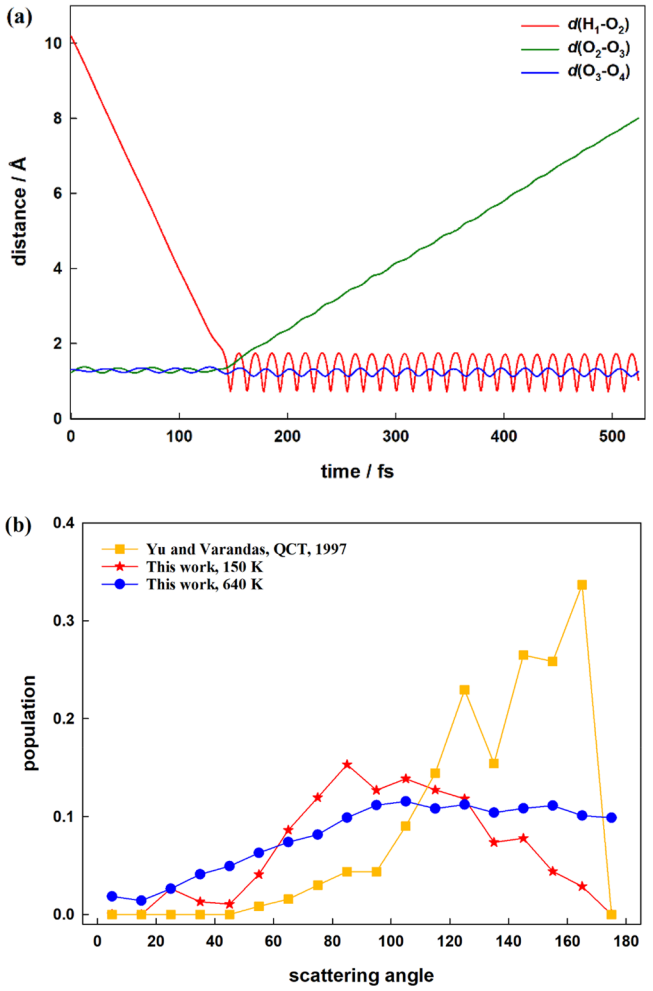

Figure 5. (a) Typical trajectory for the reaction $H + O_3 \rightarrow OH + O_2$. (b) Scattering angle distribution of products at 150 and 640 K, compared with the results of Yu et al. at E_t = 3.376 kJ/mol.

kcal/mol with an impact parameter of 1.654 Å, the product vibrational quantum numbers are $v = 9$ for OH and $v = 1$ for O_2. The large OH vibrational excitation is clearly seen in the figure as the strong oscillation of the O−H distance after the impact. Obviously, the reaction is direct and fast, without a long-lived HO_3 intermediate. The DCS is shown in Figure 5(b), in which the products are scattered in all angles. For comparison, the distribution reported by Yu and Varandas[17] is also included in the figure, which differs from the current result in that the distribution is dominated in the small scattering angles due to a rebound mechanism. Our angular distribution is much more isotropic, suggesting a mixture of several mechanisms, including rebound and stripping, depending on the impact parameter.

In summary, we explore the dynamics of the $H + O_3$ reaction and its deuterated counterpart on a recently developed accurate PIP-NN PES, in order to understand the origin of the strong vibrational excitation in the OH product. The dynamics was simulated using a quasi-classical trajectory method with two different binning approaches for determining the product vibrational quantum numbers. The dynamical calculations indicate that the reaction exoergicity is almost exclusively channeled into the vibration in the OH product, underscoring the radical departure of this reaction from the statistical limit. The calculated OH vibrational distribution is found to be strongly inverted with a peak near the highest accessible vibrational state, in excellent agreement with experiment, validating the accuracy of the PES. The theory-experiment agreement is substantially improved over the previous theoretical work, suggesting inaccuracies in the DMBE I PES used in the dynamics study of Yu and Varandas.[17] The OD vibrational distribution is also obtained, and it has similar characteristics as that of OH. This serves as a prediction for future experimental studies. More importantly, our analysis identified the dynamic origin of the nonstatistical energy disposal as the unique reaction coordinate at a small barrier in the entrance channel, which has an exceptionally large projection from the OH vibration. The elucidation of the extreme vibrational excitation of the OH product in the $H + O_3$ reaction helps to shed valuable light on the formation of OH airglow in the Meinel bands in the upper atmosphere.

Based on the previously reported PIP-NN PES for the HO_3 system,[20] all the QCT calculations were performed using the VENUS program package.[29,30] An ensemble of 120 000 trajectories was computed at each of the six different translational temperatures, T = 150, 220, 298, 360, 480, and 640 K, for both the $H + O_3$ and $D + O_3$ reactions. After testing with a small set of trajectories, the maximal impact parameter b_{max} was determined to be 3.0 Å for both reactions over the entire temperature range. The initial relative translational energy and ro-vibrational energies of reactants were sampled from the Boltzmann distribution at each temperature. Meanwhile, the impact parameter b was generated according to $b = b_{max}\zeta^{1/2}$, using a random number (ζ) ranging from 0 to 1. The time step in the propagation was selected to be 0.1 fs to converge the energy within 0.01 kcal/mol. The trajectories were initiated at a separation of 10.0 Å and terminated when products or reactants are separated by 10.5 Å.

The differential cross section (DCS) is calculated according to

$$\frac{d\sigma_r}{d\Omega} = \frac{\sigma_r P_r(\theta)}{2\pi \sin(\theta)}$$

where the reaction probability $P_r(T)$ at the specified temperature T is given by the ratio between the number of reactive trajectories (N_r) and total number of trajectories (N_{total}): $P_r(T) = N_r/N_{total}$. The scattering angle θ is defined as the angle between the velocity vectors $\vec{v}_f = \vec{v}_{OH} - \vec{v}_{O_2}$ and $\vec{v}_i = \vec{v}_H - \vec{v}_{O_3}$:

$$\theta = \arccos\left(\frac{\vec{v}_i \cdot \vec{v}_f}{|\vec{v}_i||\vec{v}_f|}\right)$$

Obviously, the angle of 180° corresponds to backward scattering, while 0° corresponds to forward scattering. Finally, the reactive integral cross section (ICS) at a given temperature is computed according to the following formula:

$$\sigma_r(T) = \pi b_{max}^2 P_r(T)$$

The product rotational quantum number can be easily derived from the diatomic rotational angular momentum

$$|\vec{j}| = \sqrt{J(J+1)}\,\hbar$$

https://dx.doi.org/10.1021/acs.jpclett.1c00159
J. Phys. Chem. Lett. 2021, 12, 1822−1828

by rounding it up to the nearest integer.

The method to determine the vibrational quantum number for the diatomic products is the Einstein-Brillouin-Keller (EBK) approach.[19] In this method, the vibrational action variable can be expressed as the semiclassical quantization of the action integral

$$n' = \oint \left\{ \frac{2\mu}{h} \left[E - V(r) - \frac{J(J+1)\hbar^2}{2\mu r^2} \right] \right\}^{1/2} \mathrm{d}r - \frac{1}{2}$$

where μ is the reduced mass, and h is Planck's constant. It is worth mentioning that the EBK semiclassical method is capable of handling anharmonicity for diatom molecules. The vibrational quantum numbers were determined from the noninteger action variables by binning. There are two binning methods, namely, the HB and GB.[31,32]

For the HB method, all the reactive trajectories are counted with the same weight with the action variable rounded to the nearest integer. The probability of the state n is thus given by

$$P_{\mathrm{HB}}(n) = \frac{N(n)}{N_{\mathrm{traj}}}$$

where $N(n)$ is the number of the products in a particular vibrational state n from the total number of the reactive trajectories (N_{traj}). The HB method allows for the population of energetically forbidden states, as classical mechanics does not observe quantization of energy levels. This shortcoming can be mitigated by the GB method, which confers a "quantum spirit".[33] Specifically, the Gaussian weight of the pth trajectory (with a noninteger classical action variable n') in a given vibrational state n is calculated by

$$G_p(n) = \frac{\beta}{\sqrt{\pi}} \exp[-\beta^2(n' - n)^2], \quad p = 1, 2, \cdots, N(n)$$

where $\beta = 2(\ln 2)^{1/2}/\delta$ is a positive real parameter. δ is the full width at half-maximum that is taken as 0.1 in this work. The Gaussian binning probability of the state n is given by

$$P_{\mathrm{GB}}(n) = \frac{\sum_{p=1}^{N(n)} G_p(n)}{N_{\mathrm{traj}}}$$

The GB method effectively removes trajectories that do not have the quantized energies, thus correcting the problems in the HB method. Since the width of the Gaussian is quite narrow, the GB method requires a large number of trajectories.

AUTHOR INFORMATION

Corresponding Author

Xixi Hu − *Kuang Yaming Honors School, Institute for Brain Sciences, Jiangsu Key Laboratory of Vehicle Emissions Control, Center of Modern Analysis, Nanjing University, Nanjing 210023, China;* orcid.org/0000-0003-1530-3015; Email: xxhu@nju.edu.cn

Authors

Qixin Chen − *Institute of Theoretical and Computational Chemistry, Key Laboratory of Mesoscopic Chemistry, School of Chemistry and Chemical Engineering, Nanjing University, Nanjing 210023, China*

Hua Guo − *Department of Chemistry and Chemical Biology, University of New Mexico, Albuquerque, New Mexico 87131, United States;* orcid.org/0000-0001-9901-053X

Daiqian Xie − *Institute of Theoretical and Computational Chemistry, Key Laboratory of Mesoscopic Chemistry, School of Chemistry and Chemical Engineering, Nanjing University, Nanjing 210023, China;* orcid.org/0000-0001-7185-7085

Complete contact information is available at: https://pubs.acs.org/10.1021/acs.jpclett.1c00159

Notes

The authors declare no competing financial interest.

ACKNOWLEDGMENTS

This work was supported by the National Natural Science Foundation of China (grant nos. U1932147 and 22073042 to X.H. and 21733006 to D.X.) and in part by the US Department of Energy (grant no. DE-SC0015997 to H.G.). We are grateful to the High Performance Computing Center (HPCC) of Nanjing University for doing the QCT calculations on its blade cluster system.

REFERENCES

(1) Meinel, A. B. OH emission bands in the spectrum of the night sky I. *Astrophys. J.* **1950**, *111*, 555−564.

(2) Meinel, A. B. OH emission bands in the spectrum of the night sky II. *Astrophys. J.* **1950**, *112* (1), 120−130.

(3) Bates, D. R.; Nicolet, M. The photochemistry of atmospheric water vapor. *J. Geophys. Res.* **1950**, *55* (3), 301−327.

(4) Herzberg, G. The atmospheres of the planets. *J. R. Astron. Soc. Canada* **1951**, *45*, 100−123.

(5) Smith, A. K.; López-Puertas, M.; Xu, J.; Mlynczak, M. G. The heating efficiency of the exothermic reaction H + O_3 in the mesosphere. *J. Geophys. Res. Atmos* **2015**, *120* (24), 12739−12747.

(6) Anlauf, K. G.; Macdonald, R. G.; Polanyi, J. C. Infrared chemiluminescence from H + O_3 at low pressure. *Chem. Phys. Lett.* **1968**, *1* (13), 619−622.

(7) Charters, P. E.; Macdonald, R. G.; Polanyi, J. C. Formation of Vibrationally Excited OH by the Reaction H + O_3. *Appl. Opt.* **1971**, *10* (8), 1747−1754.

(8) Coltharp, R. N.; Worley, S. D.; Potter, A. E. Reaction Rate of Vibrationally Excited Hydroxyl with Ozone. *Appl. Opt.* **1971**, *10* (8), 1786−1789.

(9) Spencer, J. E.; Glass, G. P. The reaction of atomic hydrogen with NO_2. *Chem. Phys.* **1976**, *15* (1), 35−41.

(10) Ohoyama, H.; Kasai, T.; Yoshimura, Y.; Kimura, H.; Kuwata, K. Initial distribution of vibration of the OH radicals produced in the H + O_3 → OH($X^2\Pi_{1/2,3/2}$) + O_2 reaction. Chemiluminescence by a crossed beam technique. *Chem. Phys. Lett.* **1985**, *118* (3), 263−266.

(11) Klenerman, D.; Smith, I. W. M. Infrared chemiluminescence studies using a SISAM spectrometer. Reactions producing vibrationally excited OH. *J. Chem. Soc., Faraday Trans. 2* **1987**, *83* (1), 229−241.

(12) Cox, J. D.; Wagman, D. D.; Medvedev, V. A. *Codata Key Values for Thermodynamics*; Hemisphere Publishing Corporation: New York, Washington, Philadelphia, London, 1989.

(13) Taniguchi, N.; Takahashi, K.; Matsumi, Y.; Dylewski, S. M.; Geiser, J. D.; Houston, P. L. Determination of the heat of formation of O_3 using vacuum ultraviolet laser-induced fluorescence spectroscopy and two-dimensional product imaging techniques. *J. Chem. Phys.* **1999**, *111* (14), 6350−6355.

(14) Ruscic, B.; Pinzon, R. E.; Morton, M. L.; Srinivasan, N. K.; Su, M.-C.; Sutherland, J. W.; Michael, J. V. Active Thermochemical Tables: Accurate Enthalpy of Formation of Hydroperoxyl Radical, HO_2. *J. Phys. Chem. A* **2006**, *110* (21), 6592−6601.

(15) Levine, R. D. *Molecular Reaction Dynamics*; Cambridge University Press: Cambridge, 2005; DOI: 10.1017/CBO9780511614125.

(16) Varandas, A. J. C.; Yu, H. G. Double many-body expansion potential energy surface for ground-state HO_3. *Mol. Phys.* **1997**, *91* (2), 301−318.
(17) Yu, H. G.; Varandas, A. J. C. Dynamics of H(D) + O_3 reactions on a double many-body expansion potential-energy surface for ground state HO_3. *J. Chem. Soc., Faraday Trans.* **1997**, *93* (16), 2651−2656.
(18) Zhang, D. H.; Guo, H. Recent Advances in Quantum Dynamics of Bimolecular Reactions. *Annu. Rev. Phys. Chem.* **2016**, *67*, 135−58.
(19) Gutzwiller, M. C. *Chaos in Classical and Quantum Mechanics*; Springer Science+Business Media New York: New York, 1990; DOI: 10.1007/978-1-4612-0983-6.
(20) Zuo, J.; Chen, Q.; Hu, X.; Guo, H.; Xie, D. Theoretical Investigations of Rate Coefficients for H + O_3 and HO_2 + O Reactions on a Full-Dimensional Potential Energy Surface. *J. Phys. Chem. A* **2020**, *124* (32), 6427−6437.
(21) Hu, X.; Zuo, J.; Xie, C.; Dawes, R.; Guo, H.; Xie, D. An ab initio based full-dimensional potential energy surface for OH + O_2 ⇄ HO_3 and low-lying vibrational levels of HO_3. *Phys. Chem. Chem. Phys.* **2019**, *21* (25), 13766−13775.
(22) Chen, Q.; Hu, X.; Guo, H.; Xie, D. Theoretical H + O_3 rate coefficients from ring polymer molecular dynamics on an accurate global potential energy surface: Assessing experimental uncertainties. *Phys. Chem. Chem. Phys.* **2021**, DOI: 10.1039/D0CP05771A.
(23) Jiang, B.; Guo, H. Relative efficacy of vibrational vs. translational excitation in promoting atom-diatom reactivity: rigorous examination of Polanyi's rules and proposition of sudden vector projection (SVP) model. *J. Chem. Phys.* **2013**, *138* (23), 234104.
(24) Guo, H.; Jiang, B. The sudden vector projection model for reactivity: mode specificity and bond selectivity made simple. *Acc. Chem. Res.* **2014**, *47* (12), 3679−3685.
(25) Habershon, S.; Manolopoulos, D. E.; Markland, T. E.; Miller, T. F., III. Ring-polymer molecular dynamics: quantum effects in chemical dynamics from classical trajectories in an extended phase space. *Annu. Rev. Phys. Chem.* **2013**, *64*, 387−413.
(26) Suleimanov, Y. V.; Allen, J. W.; Green, W. H. RPMDrate: Bimolecular chemical reaction rates from ring polymer molecular dynamics. *Comput. Phys. Commun.* **2013**, *184* (3), 833−840.
(27) Suleimanov, Y. V.; Aoiz, F. J.; Guo, H. Chemical Reaction Rate Coefficients from Ring Polymer Molecular Dynamics: Theory and Practical Applications. *J. Phys. Chem. A* **2016**, *120* (43), 8488−8502.
(28) Polanyi, J. C. Concepts in reaction dynamics. *Acc. Chem. Res.* **1972**, *5* (5), 161−168.
(29) Hu, X.; Hase, W. L.; Pirraglia, T. Vectorization of the general Monte Carlo classical trajectory program VENUS. *J. Comput. Chem.* **1991**, *12* (8), 1014−1024.
(30) Hase, W. L.; Duchovic, R. J.; Hu, X.; Komornicki, A.; Lim, K. F.; Lu, D. H.; Peslherbe, G. H.; Swamy, K. N.; Linde, S. R. R. V.; Varandas, A. VENUS96: a general chemical dynamics computer program. *J. Quantum Chem. Program Exch. Bull.* **1996**, *16*, 671.
(31) Bonnet, L.; Rayez, J. C. Quasiclassical trajectory method for molecular scattering processes: necessity of a weighted binning approach. *Chem. Phys. Lett.* **1997**, *277* (1), 183−190.
(32) Bonnet, L.; Rayez, J.-C. Gaussian weighting in the quasiclassical trajectory method. *Chem. Phys. Lett.* **2004**, *397* (1−3), 106−109.
(33) Bonnet, L. Classical dynamics of chemical reactions in a quantum spirit. *Int. Rev. Phys. Chem.* **2013**, *32* (2), 171−228.

https://dx.doi.org/10.1021/acs.jpclett.1c00159
J. Phys. Chem. Lett. 2021, 12, 1822−1828